Field- and Gaussian-based 3D-QSAR studies on barbiturate analogs as MMP-9 inhibitors

ARTICLE *in* MEDICINAL CHEMISTRY RESEARCH · NOVEMBER 2013

Impact Factor: 1.4 · DOI: 10.1007/s00044-013-0479-6

3 AUTHORS, INCLUDING:

Sukesh Kalva
University of KwaZulu-Natal
13 PUBLICATIONS **22** CITATIONS
SEE PROFILE

Vinod Devaraji
Schrodinger
20 PUBLICATIONS **36** CITATIONS
SEE PROFILE

Med Chem Res
DOI 10.1007/s00044-013-0479-6

MEDICINAL CHEMISTRY RESEARCH

ORIGINAL RESEARCH

Field- and Gaussian-based 3D-QSAR studies on barbiturate analogs as MMP-9 inhibitors

Sukesh Kalva · D. Vinod · Lilly M. Saleena

Received: 17 July 2012 / Accepted: 9 January 2013

Abstract Matrix metalloproteinase-9 (MMP-9) is one of the important enzymes belongs to gelatinase family and involved in multiple cellular processes including proliferation, angiogenesis, and metastasis. Various studies show that *N*-substituted homopiperazine barbiturates are promising and also selective for the MMP-9 inhibition. In this study, we selected and reported 49 barbiturate derivatives as inhibitors of MMP-9 and performed structure-based 3D-QSAR studies to elucidate the important structural features responsible for binding affinity. Crystal structure of MMP-9 complexed with barbiturate available in PDB was selected and performed quantum-polarized ligand docking for the reported inhibitors. Receptor-based alignment obtained from the docked poses were used for field- and Gaussian-based 3D-QSAR study. The results of both field and Gaussian models gave the good predictive correlation coefficient (test set) q^2 of 0. 77 and 0.85, and the conventional correlation coefficient (training set) r^2 of 0.845 and 0.928, respectively. The results of 3D-QSAR and docking studies validate each other and provided insight into the structural requirements for MMP-9 inhibition. The outcomes of the contour maps for both steric and Gaussian models results indicate that steric and hydrophobic interactions are major contributing factor for the activity and these findings will be useful to design the new inhibitors against MMP-9.

Keywords Gelatinases · *N*-Substituted homopiperazine barbiturate derivatives · Quantum-polarized ligand docking · 3D-QSAR

Electronic supplementary material The online version of this article (doi:10.1007/s00044-013-0479-6) contains supplementary material, which is available to authorized users.

S. Kalva · L. M. Saleena (✉)
Department of Bioinformatics, SRM University, SRM Nagar, Kattankulathur- 603203, Kancheepuram District, Chennai, India
e-mail: lmsaleena@yahoo.com; lmsaleena@ktr.srmuniv.ac.in

D. Vinod
College of Pharmacy, Madras Medical College, Chennai 600003, India

Introduction

Cancer metastasis is the major cause of death in various cancer patients (Weinstat and Steeg, 1994; Giannelli and Antonaci, 2002). During metastasis, extracellular matrix (ECM) components of the basement membrane are degraded by various proteinases thereby facilitating the detachment of tumor cells from the basement membrane and crossing the various tissue compartments (Marina and Ivan, 2007). The major functional contributors which have long been associated with metastasis are matrix metalloproteinases (MMPs) (Chambers and Matrisian, 1997). MMPs have been classified into five subfamilies based on the substrate specificity and primary sequence similarities. They are gelatinases, elastin, collagenases, stromelysins, and membrane type MMPs (Murphy *et al*., 2002). Gelatinases (MMP-2 and MMP-9) are major enzymes which are involved in the tumor invasion and metastasis. These enzymes are directly involved in cancer metastasis by degrading the type IV collagen, breached by tumor cells during metastasis (Klein and Bischoff, 2011).

Among MMPs, gelatinase B or MMP-9 represents the largest and most complex member majorly linked with the cancer (Liu *et al*., 2010). It is synthesized and secreted as proenzyme, which remains inactive unless it undergoes proteolytic cleavage. Different proteases are also known to activate gelatinase B, for e.g., plasminogen activator by

Published online: 15 February 2013

converting into plasmin, an activator for different MMPs. These MMPs activate the other MMPs finally leading to the activation of gelatinase B. Many growth factors and cytokines found to stimulate the production of MMPs especially gelatinase B (Van den Steen *et al*., 2002). Gelatinase B is an interesting and important target for inhibition since it is reported as a mediating enzyme in many disease states, for e.g., acute inflammation, cardiovascular diseases, cancer, neuropsychiatric disorders, and multiple sclerosis (Rybakowski, 2009). Besides their role in pathological diseases they are also involved in various physiological processes like angiogenesis, connective tissue remodeling (Loffek *et al*., 2011). Elevated expression of MMP-9, along with MMP-2 is involved in oral squamous cell carcinoma, breast, lung, colon, ovarian, and gastric carcinoma (Schmalfeldt *et al*., 2001; Illemann *et al*., 2006; Singer *et al*., 2002; Zheng *et al*., 2010; Kim *et al*., 2009). Recent studies report that an increased activity of MMP-9 system result in pathogenesis of schizophrenia, coronary artery disease, which is confirmed by molecular genetic studies of fucntional −1,562 c/t polymorphism of MMP-9 gene (Rybakowski *et al*., 2009). Significantly, MMP-2 and MMP-9 deficient mice exhibited the suppression of tumor growth and metastasis without developing any gross abnormalities (Tamura *et al*., 1998). Since there is a close similarity in the overall three-dimensional structure of MMP family of proteins the concept of designing a selective inhibitors is a difficult task (Rao, 2005). Over the past years, MMP inhibitors clinical trials conducted in cancer patients were unsuccessful to show a significant therapeutic response, it was because the majority of patients registered had advanced metastasis disease. In fact the use of broad spectrum MMP inhibitors in clinical trials was greatly limited by musculoskeletal syndrome side effects (Nuti *et al*., 2011). Since compounds failed, blocking the MMP-9 activity by more specific inhibitors might be of therapeutic benefit, in particular in patients with early stage cancers (Tandon and Sinha, 2011). In 2001, Hoffman La Roche reported barbiturates are the inhibitors of MMPs with good gelatinase selectivity (Wang *et al*., 2011). These novel barbiturates show selective inhibition against gelatinases and this motivated to select this inhibitors to reveal the selectivity profile against MMP-9 this can give clear picture on designing of molecules selectively towards MMP-9. Present 3D-QSAR methods have done tremendous advancement in lead discovery and optimization of chemical analogs against different activity (Peterson *et al*., 2009; Bairy *et al*., 2009; Nayana *et al*., 2008). To uncover the important structural features responsible for the higher activity against MMP-9, we have performed 3D-QSAR studies on barbiturate analogs.

MMP-9 is a zinc binding protein, the atoms of receptor and ligand are polarized while interacting with the zinc metal (Jain and Jayaram, 2007). This polarization effect cannot be accounted when we use normal docking methods because of their mechanic force fields. Hence, for accurate calculation of polarized charges of these atoms we have used quantum-polarized ligand docking (QPLD), available in Schrodinger software (methodology was discussed in "Materials and methods" section). Previous QPLD docking studies had shown its superiority compared to other docking programs in the study case of 40 protein–ligand complexes with root-mean-square deviations (RMSDs) of docked pose to native pose in most cases less than 1.00 Å (Sabbah *et al*., 2012; Cho *et al*., 2005). In case of our protein with this method we got a very good reproducibility with co-crystal ligand (PDB ID: 20VX). We docked all the 49 compounds using QPLD and generated the alignment from the best ranked poses of the docking result which is for crucial for generating a highly predictive 3D-QSAR.

Though many different hydroxamate, non-hydroxamate, phosphonic, and other similar inhibitors have been synthesized and experimentally assessed, to the best of our knowledge, no QSAR or 3D-QSAR (three-dimensional quantitative structure–activity relationship) investigations for such kind of compounds has not been reported till date (Georgiadis and Yiotakis, 2008). This study aims to build predictive 3D-QSAR models by using field- and Gaussian-based methods, and using them to find the correlation between the structure of *N*-homopiperazine derivatives and activities to design more potent and selective inhibitors. These two methods sample the potential fields surrounding a set of ligands and construct 3D-QSAR models by correlating these 3D fields with the corresponding experimental activities of ligands interacting with a receptor.

Materials and methods

Dataset collection

A total number of 49 MMP-9 inhibitors which showed single digit nano-molar potency and selectivity between gelatinases (gelatinases A and B) in fluorogenic assay were collected from the recent literature (Wang *et al*., 2011). The in vitro bioactivities of the inhibitors selected were reported to inhibit MMP-9 by 50 % (IC_{50}). The IC_{50} values were converted into negative logarithm of IC_{50} (pIC_{50}) ($pIC_{50} = 9 - \log 10(IC_{50})$). All the compounds with pIC_{50} values ranging from 6.15 to 8.95 nM were used in this study (Supplementary Table S1). The 2D structure of the compounds was built using ISIS Draw program (Li *et al*., 2004) The geometry for all these molecules was converted into 3D structure using Maestro 9.2 version (Schrodinger, version 9.2, 2011, LLC, Portland, OR). The 3D structure of the molecules was processed with LigPrep module using the following parameters (i) the force field used was OPLS 2005, (ii) all possible ionization states at biological pH,

Table 1 Actual and predicted IC_{50} values for the training and test set of 49 compounds

S. no	Molecule number	Experimental IC_{50} values (nM)	Experimental pIC_{50} values (nM)	Predicted IC_{50} values (field)	Predicted IC_{50} values (Gaussian)
1	8C[a]	10	8.001	7.825	7.689
2	8D	15	7.824	8.112	7.946
3	8G[a]	86	7.066	7.138	7.186
4	8I[b]	16	7.796	7.973	7.734
5	8 J[a]	9.4	8.027	8.155	8.16
6	9A[c]	1.1	8.959	8.242	8.579
7	9B	22	7.658	7.783	7.870
8	9C	2.9	8.538	7.861	8.387
9	9D[a]	7.5	8.125	8.036	8.091
10	12A	73	7.137	7.000	7.454
11	12B	45	7.347	7.305	7.298
12	12C	54	7.268	7.328	7.177
13	13A	13	7.886	8.050	7.849
14	13B[c]	16	7.796	7.631	7.734
15	13C[a]	9.8	8.009	7.597	7.906
16	13D	104	6.983	6.899	7.159
17	14	13	7.886	7.753	8.017
18	15	29	7.538	7.577	7.360
19	16	269	6.570	6.650	6.339
20	17	60	7.222	7.262	7.299
21	18	50	7.301	7.642	7.220
22	19[b]	329	6.483	6.483	6.238
23	20	86	7.066	6.949	7.114
24	21[c]	264	6.578	7.294	6.375
25	22[b]	2.55	8.593	8.002	8.000
26	23	308	6.511	6.611	6.308
27	24	24	7.620	7.755	7.410
28	25	30	7.523	7.322	7.410
29	26	47	7.328	7.496	7.480
30	27	106	6.975	7.144	6.806
31	28[a]	264	6.578	6.543	7.055
32	29	80	7.097	7.119	7.307
33	30[a]	268	6.572	6.536	6.844
34	31[a]	23	7.638	7.784	7.583
35	32	31	7.509	7.390	7.440
36	33	95	7.022	7.113	6.988
37	34[a]	100	7.000	7.382	7.263
38	35	25	7.602	7.772	7.620
39	36[a]	25	7.602	7.508	7.620
40	37[c]	311	6.507	7.351	6.516
41	38[c]	411	6.386	6.578	6.620
42	39	24	7.620	7.717	7.631
43	40	706	6.151	6.149	6.069
44	41	681	6.167	6.163	6.370
45	42	20	7.699	7.607	7.589
46	43	83	7.081	7.012	7.116
47	44	54	7.268	6.970	7.236
48	45	142	6.848	6.753	7.015
49	46	184	6.735	6.713	6.913

[a] The test set molecules in both field and Gaussian models

[b] The test set molecules in Gaussian-based model

[c] The test set molecules in field-based model

Remaining all are training set molecules in both field and Gaussian models

(iii) possible tautomers, sterospecificity, and the original stereochemistry of the compounds were generated depending upon the number of chiral centers, and (iv) one low energy ring conformation per ligand were generated (Macro Model, version 9.9, Schrödinger, LLC, New York, NY, 2012, Jorgensen and Maxwell, 1996). QPLD, field- and Gaussian-based 3D-QSAR calculations were performed for all the molecules using Schrodinger 9.2v. All the training and test set molecules with experimental and predicted IC50 values were listed in Table 1.

Alignment procedure

Alignment of molecules is the most crucial input for generation of field-based 3D-QSAR models. In this study, a QPLD docking was performed to generate a receptor-based alignment to incorporate quantum mechanical charges for all the ligands. By using this method a very good binding mode and alignment of ligands with receptor active site was obtained were almost similar to the co-crystal ligand 4MR which was seen in one of the MMP-9 receptors (PDB ID: 2OVX). Figure 1a, b shows barbiturate derivatives aligned with co-crystal ligand in the active site of MMP-9 receptor.

Protein preparation

Protein structure (PDB ID: 2OVX) (http://www.rcsb.org/pdb/) was prepared using protein preparation wizard workflow of Schrodinger 9.2v. All the water molecules were removed, followed by H-bond optimization with the side chain structures of Gln and Asn. After implementing necessary optimization to the structure, the protein was subsequently minimized using OPLS 2005 force field using heavy atom convergence of 0.5 Å.

Receptor grid generation

The protein processed in the previous step was used to define the receptor site by using receptor grid generation of Schrödinger 9.2v. Grid files represent physical properties of a spatial arrangement of the receptor (specifically the active site) that are searched while performing docking. The receptor grid was generated by selecting the centroid

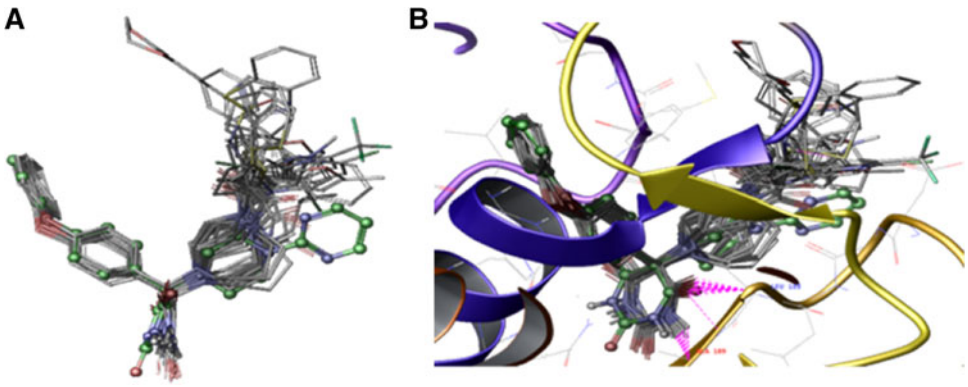

Fig. 1 **a** Some of the aligned molecules with co-crystal ligand 4MR (*balls* and *stick*) obtained using QPLD alignment and **b** QPLD alignment of some molecules sharing H-bond interactions (*pink dotted lines*) with active site of MMP-9 (PDB ID: 2OVX) (Color figure online)

of the crystal ligand 4MR in the MMP-9 receptor (PDB ID: 2OVX) in which the rotation of the receptor hydroxyl and thiol groups in the active site was allowed and the van der Waals radii scaling for non-polar parts of the receptor was set with a scaling factor of 0.8 and the partial charge cutoff to 0.25 to increase active site flexibility.

Ligand docking using QPLD

We used QPLD (QM-polarized ligand docking) workflow, available as in the Schrodinger suite, for QM/MM docking implementation. QPLD is an improved docking method that incorporates quantum mechanical and molecular mechanical (QM/MM) calculations (Cho *et al*., 2005). QPLD docking is a semi rigid docking method where ligand is completely flexible whereas the receptor site is softened by adjusting the van der Waals scaling which allows the rotation of the rotatable amino acid residues in active site. QPLD protocol involves combined algorithm of Glide and the QSite programs in the Schrödinger suite. The QPLD algorithm begins with a Glide docking job that generates several geometrically unique protein–ligand complexes. QSite then performs a single-point energy calculation on each complex, treating the ligand with ab initio methods and deriving partial atomic charges using 3-21G basis set with BLYP (Becke's exchange potential and Lee–Yang–Parr correlation functional) density function. Glide then re-docks the ligand using each of the ligand charge sets calculated by QSite, and the QPLD algorithm returns the most energetically favorable pose. Finally, the pose which is close enough to crystal structure was chosen for performing the 3D-QSAR calculations.

Field- and Gaussian-based 3D-QSAR model energy calculations

3D-QSAR analysis using field- and Gaussian-based methods was performed using field-based QSAR tool of Schrodinger 9.2 version. 3D-QSAR method is used for constructing the model by relating the known activities and 3D characteristics of set of aligned molecules (Kyaw and Xiang-Qun, 2010; Verma *et al*., 2010). A steric and electrostatic field around the ligand molecule in a three-dimensional grid was calculated using field-based 3D-QSAR. Field-based QSAR model is an alignment-dependent method in which molecular field interaction energy terms are correlated with biological activities/responses using multivariate statistical analyses. In Gaussian, 3D-QSAR model interaction energy calculations were performed using steric, electrostatic, hydrophobic, hydrogen bond donor (HBD), and hydrogen bond acceptor (HBA) potential fields and it uses Gaussian equations for field calculations.

Partial least square (PLS) analysis

pIC_{50} values were used as dependent variables and field and Gaussian intensities as descriptors were used as independent variables in the PLS regression analysis to generate 3D-QSAR models.

Workflow for 3D-QSAR model generation

3D-QSAR model generation primary requirement is the alignment of all the molecules. All the barbiturate analogs were prepared to get the appropriate binding orientation of *N*-homopiperazine barbiturates using Ligprep. Molecular docking program QPLD was employed to generate the lowest energy conformations for all the inhibitors and it gives 357 diverse conformations. Molecules were aligned based on the similar interactions and conformations of co-crystal ligand (4MR) which are present in the PDB ID: 2OVX. Finally, the lowest energy conformations for 49 molecules which have quantum mechanics charges with proper alignment and high glide score were shortlisted to generate field- and Gaussian-based 3D-QSAR models. The workflow for 3D-QSAR model generation is shown in Fig. 2.

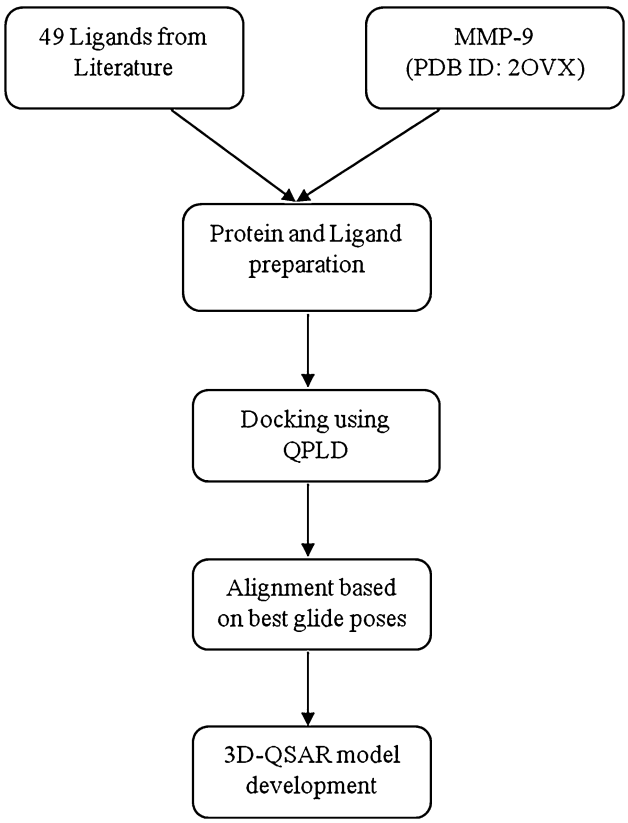

Fig. 2 Work flow for 3D-QSAR model generation

Results and discussion

QPLD

To incorporate the polarization effects of zinc metal of MMP-9 on 49 inhibitors during docking, QPLD method was used. The accuracy of QPLD in pose reproducibility was performed by re-docking the barbiturate inhibitor (4MR) co-crystallized in MMP-9 (PDB ID: 2OVX) and calculated the RMSD of the docked ligand pose with respect to the experimental binding pose. QPLD accurately reproduced the native conformation of the 4MR with very low RMSD (0.6 Å) between the docked pose and experimental binding pose and also all the important interactions made by the experimental pose (Supplementary Fig. S1). As QPLD is successful in reproducing the native pose we used QPLD for docking all the 49 inhibitors into MMP-9. The binding mode with high glide score for each compound was selected and superimposed to generate receptor-based alignment. Figure 1b shows the alignment of the poses of 49 ligands in the active site of MMP-9 receptor.

Field- and Gaussian-based QSAR model generation

One of the prerequisites for generating a highly predictive 3D-QSAR model is the alignment of compounds which were used in the study. There are several alignment methods reported among them receptor-based alignment comparatively generates best model (Aparna *et al*., 2006; Murumkar *et al*., 2010). We considered the receptor-based alignment obtained from QPLD to generate both field and Gaussian QSAR models in order to establish the statistical correlation of activity against chemical features, and to understand biological role of each fragment in the structure with the activity. Field-based 3D-QSAR model was generated with two features steric and electrostatic, whereas Gaussian model with five features including Gaussian steric, Gaussian electrostatic, HBA, HBD, and Gaussian hydrophobic. For generating and validating the models, the total inhibitors were classified into training and test set. For selecting the best possible training set, a manual clustering was done on the structural variations in the substitutions: molecule **37** with (dimethylaminonaphthalene-4-yl-sulfonyl), *S*-**40** (dihy drobenzo[1,4]dioxine-6-sulfonamido-3-methyl butyryl), **22** (3-methyl-benzopurane-2-carbonyl), **39** (methyl-1*H*-indazole-3-carbonyl), **23** (3-chloro-benzothiophene-2-carbonyl), *R*-**41** (benzo-d-thiazol-2-yl-2-methyl-2-phenyl propanoyl), and **36** (morpholine-4-carbonyl). Placing these molecules equally in the training and test set a reasonable field-based 3D-QSAR models were obtained. PLS analyses with all 35 compounds for field-based model and 37 compounds for Gaussian model in the training set with 5 PLS factors afforded models with good r^2 and q^2 values. The experimental and predicted IC_{50} values for the training and test molecules for both the models are given in Table 1.

Field-based 3D-QSAR model

With the help of PLS with five factors the field-based 3D-QSAR was generated by correlating with steric and electrostatic field intensities of the training set. An r^2cv value of 0.58 was derived from the leave one out (LOO) cross-validation method and non-cross-validation analysis yielded an r^2 value of 0.84 with a standard error of estimate of 0.13 and an F ratio of 71.7. The statistical summary of the model was listed in Supplementary Table S2. The steric and electrostatic contributions for this model were found to be 0.66 and 0. 33. This signifies that the steric field is more important than the electrostatic groups for protein–ligand interactions. The contribution (%) of steric and electrostatic field intensities is given in Table 2. For the model validation, 15 testing-set inhibitors were used and predicted pIC_{50} values were calculated. The predictive correlation coefficient, q^2 value was 0.77 indicating that these models had reasonably good predictive power.

Steric contour maps

The field-based steric interactions are represented by green and yellow colors, where green regions in the molecule

Table 2 Summary of results obtained using field- and Gaussian-based 3D-QSAR models

PLS statistics	Field	Gaussian
SD	0.130	0.175
r^2	0.845	0.928
r^2cv	0.582	0.563
r^2 scramble	0.896	0.854
q^2	0.771	0.85
Field contributions (%)		
Steric	0.66	0.44
Electrostatic	0.33	0.08
Hydrophobic		0.31
HBA		0.15
HBD		0.02

SD standard deviation of the regression, r^2 non-cross-validated correlation coefficient, r^2cv cross-validated correlation coefficient, q^2 LOO cross-validated correlation coefficient, *HBA* H-bond acceptor, *HBD* H-bond donor

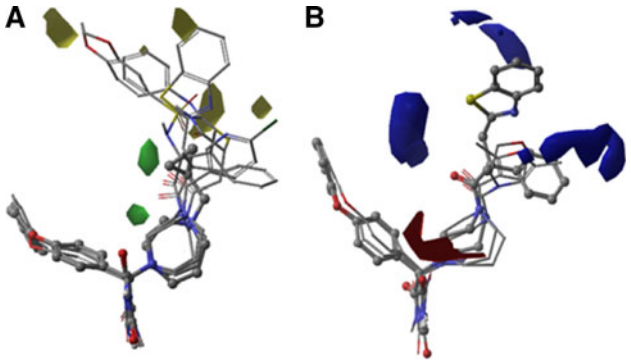

Fig. 3 **a** Steric contour and **b** electrostatic contour maps for the best field-based 3D-QSAR model. In **a**, active molecules were shown in *balls* and *sticks* and inactive molecules were represented as *sticks*. For steric field, favorable regions are in *green* and disfavored regions are in *yellow*. In **b**, active molecules were shown in *sticks* and inactive molecules were represented as *balls* and *sticks*. For electrostatic, favorable electropositive regions are in *blue* and favorable electronegative regions are in *red* (Color figure online)

represent that addition of bulky substituents may increase the activity while bulky groups in the yellow region may reduce the activity. In the highly active molecule (**9A**) green color near the phenyl ring (cyclopropylmethyl), and closer to the piperazine ring which indicates that the presence of bulky groups or bulky substituents may favor the activity and yellow color near the piperazine and homopiperazine ring suggest that bulky substituents at that position may decrease the activity. This trend is observed in the active piperazine and homopiperazine ring analogs **9D**, **8C**, **8J**, and **8D**. This is opposite for the inactive molecules where yellow contour closer to the molecules **13D**, *S*-**46**, *R*-**41**, and *S*-**40** substituted with chloropyridine, thiozolidin, benzothiazol, and benzo dioxone suggest that increased steric bulk at that position is unfavorable which is shown in Fig. 3a. In Fig. 3a, active compounds were represented as balls and sticks and inactive molecules were represented as sticks.

Electrostatic contour maps

Figure 3b shows field-based electrostatic interactions which are represented by red and blue colors. Blue color regions in the molecule represent that electropositive groups may increase the activity while red regions represent that electronegative group may increase or enhance the activity. In homopiperazine analogs, large red contour around the amino group of homopiperazine suggests that electronegative atoms at that position may enhance the activity. In the least active molecule (*R*-**41**), blue contours mapped on the 2nd and 5th position of phenyl ring suggests that electropositive charges at that position may enhance the activity. In the moderately active compounds **24** and **36**, blue contours closer to the methyl furan 3 carbonyl and morpholine 4 carbonyl suggests that electropositive atoms at that position may enhance the activity. In Fig. 3b, inactive molecules are represented as balls and sticks and active compounds were represented as sticks.

Gaussian-based 3D-QSAR model

With the help of PLS with five factors, the Gaussian-based QSAR was generated by correlating with five field's steric, electrostatic, hydrophobic, HBD, and HBA. An r^2cv value of 0.56 were derived from the LOO cross-validation method and non-cross-validation analysis yielded an r^2 value of 0.93 with a standard error of estimate of 0.17 and an *F* ratio of 78.0. The statistical summary of model is listed in Supplementary Table S3. The contributions of the steric, electrostatic, hydrophobic, HBD, and HBA fields were 0.44, 0.08, 0.31, 0.15, and 0.022, respectively (Table 2). The field contributions of steric (0.44) and hydrophobic (0.31) intensities were higher when compared to the electrostatic, HBA, and HBD, which indicate that more requirement of steric and hydrophobic for protein–ligand interactions. Field-based model also showed similar field contribution for the generated model. The predicted IC_{50} values are given in Table 1, and contribution of five different field intensities is given in Table 2.

Gaussian steric contour maps

Figure 4a shows the contour map where steric interactions were represented by green and pink colors. Green regions

on the molecules represent favorable affect of bulky substituents, i.e., bulky groups at these positions increase the activity. Further, the bulky groups in the pink region may reduce the activity. A single carbon and methyl substitution in 4th position of homopiperazine than piperazine ring analogs shows higher activity than multiple carbon substitution or aromatic groups. From this the major role of carbon length with respect to the activity is understood. For example, compound **9A** a green contour closer to cyclopropyl methyl favors the activity. This trend was observed with the highly active molecules **8I**, **9C**, **13A**, **8D**, and **14** with substitution like cyclopropylmethyl, cyclopropylcarbonyl, acetyl, and methyl, and cyclobutane carbonyl. This is opposite for the moderately and least active molecules with heavy groups or multiple carbon substitution. For example compound **15**, the pink contour closer to the phenylthioacetyl ring which suggests that increased steric bulk is unfavorable at that position. This trend is observed for the compounds **32**, *S*-**40**, and **37** with heavy groups like phenyl proponyl, dihydrobenzoyl-1,4-dioxine-6-sulfonamido-3-methyl butyrl and dimethyl amino naphthalene-4yl-sulfonyl. The highly active molecules in Fig. 4a are represented as ball and sticks and inactive molecules were represented as sticks.

Gaussian electrostatic contour maps

Figure 4b elaborates on electrostatic contours with blue contours in the molecule represent that electropositive groups may increase the activity while red regions represent that electronegative group may enhance the activity. The contribution of electrostatic is 0.082. In general, in all the compounds red color in the 4th position of homopiperazine and piperazine indicates that electronegative groups at that position are required to enhance the activity of the molecule. For instance, in the active molecule **13a** (IC_{50}: 7.886) red contour mapped to the nitrogen atom in the homopiperazine ring suggests that electronegative charges at that position may enhance the activity and blue color closer to cyclopropyl methyl suggest that positive charges at that position may favor the activity. In inactive molecule **12b** (IC_{50}: 7.347) red contours embedded in the cyano benzoyl group denote regions of preferential negatively charged substituents while blue contour near the oxygen atom suggests electropositive substituents at that position may enhance the activity. In the moderately active compounds (**26** IC50: 7.328 and **36** IC 50: 7.602) blue color region near the sulfur, oxygen atoms suggest that replacement of electron donating groups at that position

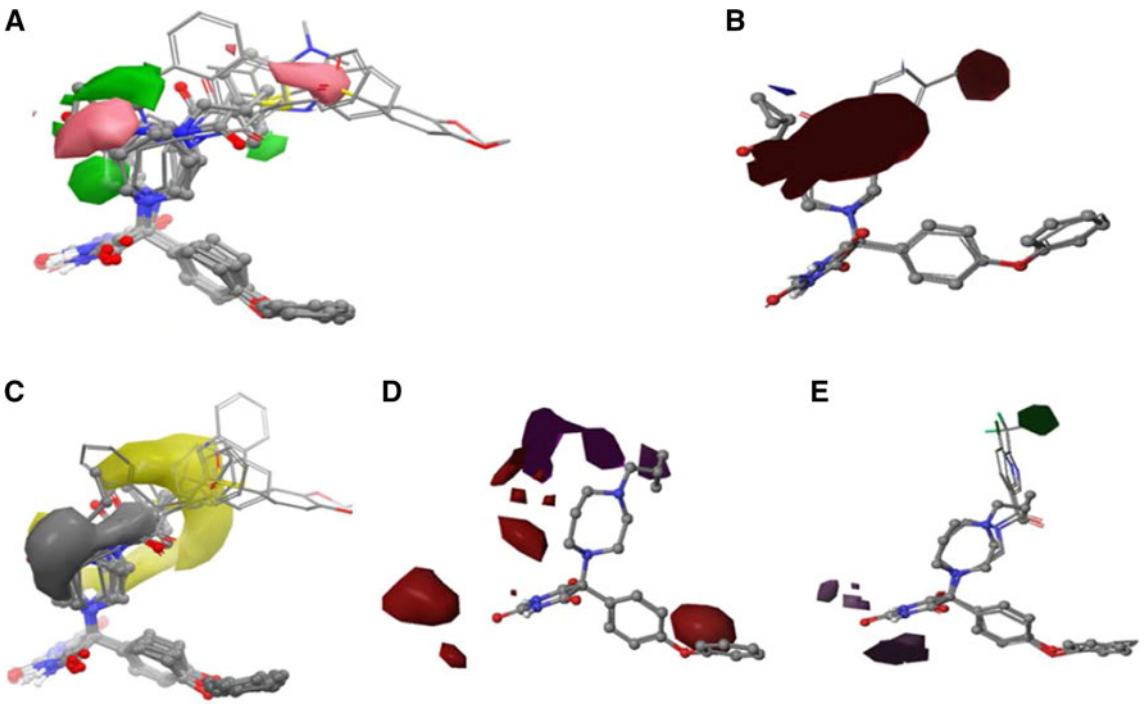

Fig. 4 Contour maps obtained for the best Gaussian-based 3D-QSAR model. **a** For Gaussian steric favored regions are in *green* and disfavored regions are in *pink*. **b** For gaussian electrostatic favorable electropositive regions are in *blue* and favorable electronegative regions are in *red*. **c** For gaussian hydrophobic, the *yellow* regions indicate favorable hydrophobic interactions and *grey* regions indicate that unfavorable hydrophobic interactions. **d** For HBA, *red* regions indicate that favorable hydrogen bond acceptor interactions and *magenta* region indicates that unfavorable hydrogen bond acceptor interactions. **e** For HBD, *blue violet* regions indicate that favorable hydrogen bond donor interactions and *green* regions indicate that unfavorable hydrogen bond donor interactions. Active molecules were represented as *balls* and *sticks* while inactive molecules were shown in *sticks* (Color figure online)

may enhance the activity. Blue color indicates that substitution of electron donating groups like alkyl groups or aliphatic groups in the beta and gamma position of phenyl ring may enhance the activity for the compounds (**15** IC_{50}: 7.538, **31** IC_{50}: 7.638, **32** IC_{50}: 7.509, and **9b** IC_{50}: 7.658).

Gaussian hydrophobic contour maps

In Fig. 4c, grey contour in the hydrophobic plot indicates that hydrophobic groups at those regions are disfavored. A yellow color contour indicates that hydrophobic groups are tolerated at that position. Grey contours which is non-hydrophobic favorable regions clearly shows the abundance of piperazine and homopiperazine derivatives in that position which can be the primary reason in all analogs the activity to fall but the homopiperazine is better than piperazine because of the extra carbon in the ring which is enclosed in the grey contours from we can conclude that a homopiperazine analogs is better which is clearly indicated with the molecule **8C**, **8D**, **8I**, **8J**, **9A**, **9C**, **9D**, **13A**, and **14**. A yellow contour closer to the methyl-substituted hydrophobic derivatives in the 4th position of homopiperazine, and piperazine ring has better activity which can be found in the molecules **8C**, **8D**, **8I**, **8J**, **9A**, **9C**, and **9d**. Whereas incremental bond length in the same position decrease the activity in the molecules which is clearly shown in the molecules **15** (phenyl thioacetyl), **18** (cyclopentane propanoyl), **32** (phenyl propanoyl), **33** (4 chlorophenyl acetyl), **34** (2 cyclohexa acetyl), *S*-**40** (dihydrobenzo[1,4]dioxine-6-sulfonamido 3-methyl butyryl), and *R*-**41** (benzo-d-thiazol-2-yl-2-methyl-2-phenyl propanoyl) which exceeds hydrophobic contour regions. The hydrophobic contribution was 0.309 in our model.

Hydrogen bond acceptor (HBA) contour maps

Figure 4d shows the HBA contour maps. The red contour in the HBA indicates that HBA groups lead to the improved activity whereas magenta contour indicates the presence of HBA groups lead to reduced activity. In general, in all the molecules the pyrimidine 2,4,6-trione is very much responsible in establishing hydrogen bonds with the Leu 188. A red contour near the phenoxy phenyl and around trione suggests that the subunit bearing HBAs will increase activity, whereas red and magenta regions indicate that addition of HBA groups at the homopiperazine ring may maintain the activity while magenta regions mapping the cyclopropylmethyl ring may reduce the activity (**9A** IC_{50}: 8.959).

Hydrogen bond donor (HBD) contour maps

Figure 4e shows the HBD contours where areas favored by donors are shown in blue violet, and unfavorable areas are shown in green color. In the entire homopiperazine and piperazine analogs, blue violet region is seen near the gamma position and around the trione ring which suggests that HBD are favored at that position. These results are correlating with the QPLD where the amino group is involved in donating the hydrogen bonds with the Ala 189. Triflurobenzoyl and chlorobenzoyl closer to the green contour suggests that they are inactive in the molecules **13d** and **28**. However, for the highly active molecules (>8.00 nM) the green contour is very far which indicates that they are highly active.

Validation of field- and Gaussian-based 3D-QSAR models

The plots of predicted versus actual binding affinities for both the training and test set inhibitors are shown in Figs. 5 and 6 which represents field- and Gaussian-based 3D-QSAR models. The predicted correlation coefficients (r^2) are 0.845 for field-based model and 0.928 for Gaussian model which indicates that Gaussian model prediction is

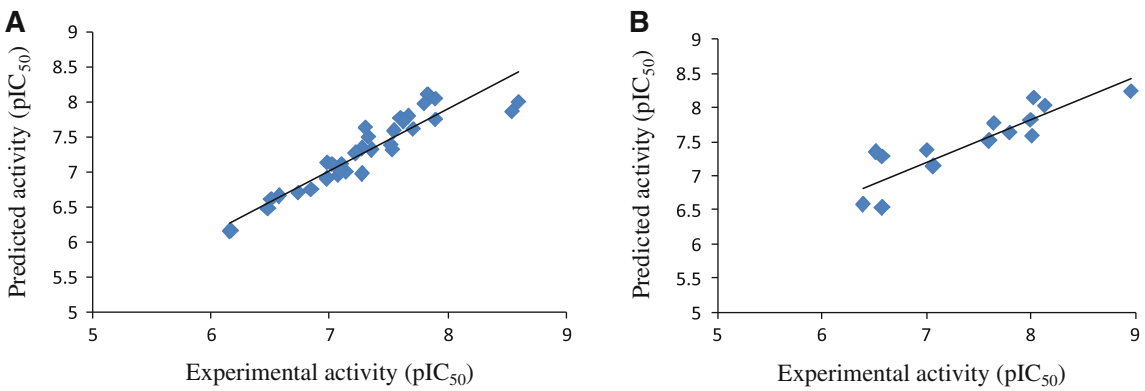

Fig. 5 Relation between experimental and predicted MMP-9 inhibitory activity values of **a** training set and **b** test set molecules using field-based 3D-QSAR model

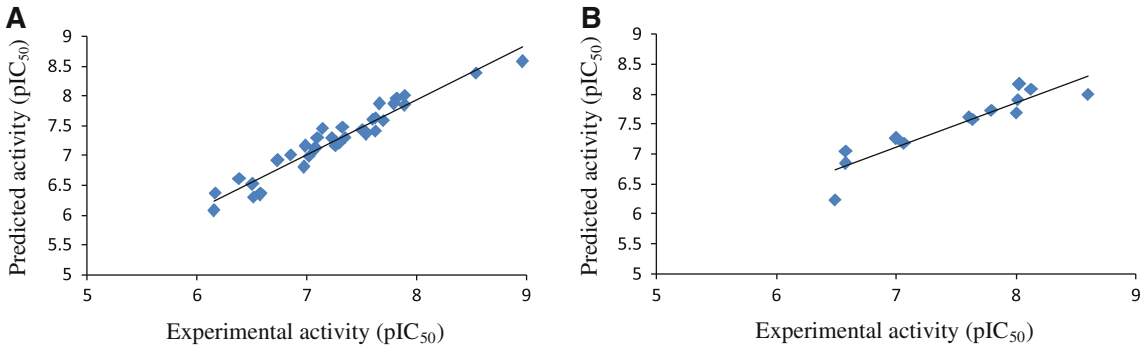

Fig. 6 Relation between experimental and predicted MMP-9 inhibitory activity values of **a** training set and **b** test set molecules using Gaussian-based 3D-QSAR model

good than the field based. By comparison of experimentally observed and predicted IC_{50} values of *N*-homopiperazine inhibitors, it can be seen that Gaussian model performed well in the prediction of activities for both training and test molecules.

After the analysis of the statistical parameters for best field and gaussian 3D-QSAR models, we concluded that both models show strong predictability and provide detailed information about the chemical features of the ligands, which will contribute to antagonistic potency against MMP-9. Figure 7 illustrates the positive and negative activity coefficient of the above core structure against MMP-9 inhibition by using following chemical features: (i) electronegative group (pink color) in position 2 of piperazine ring gives positive activity, (ii) a hydrophobic and steric groups at R1 position (light green and dark green) favors towards activity, and (iii) HBA (red) at pyrimidone 4th and 6th carbonyl position and HBD (blue) at 1st and 3rd position of the pyrimidone trione contribute towards activity. Interestingly, the contour map analysis

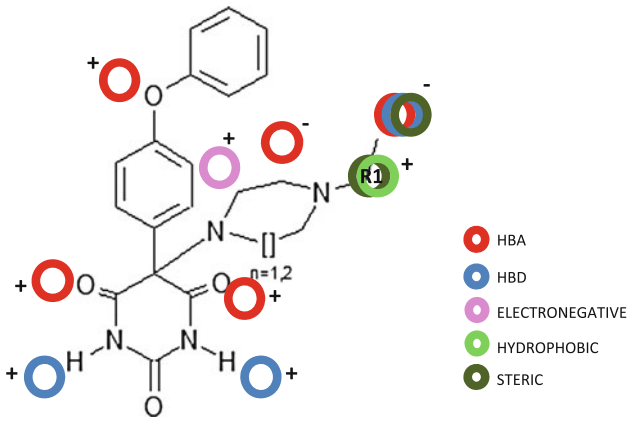

Fig. 7 Structural requirements of barbiturate derivatives for MMP-9 activity and selectivity based on the analysis of field- and Gaussian-based contour maps. In Figure, *plus* possible favorable substituent's for MMP-9 inhibitory activity and *minus* possible non-favorable substituent's for MMP-9 inhibitory activity

revealed that substitution of HBA in the 3rd position of piperazine ring and multiple carbon and aromatic group (HBA, HBD, and steric) substitutions in 4th position of homopiperazine ring will lead to decrease in activity coefficient against MMP-9 inhibition. The literature data as well as this study concludes that (HBA) substituents at 4th and 6th and (HBD) substitution at 1st and 3rd in the pyrimidone trione ring plays a essential role in MMP-9 antagonistic activity which helps us in suggesting the substituent's to improve the biological activity and selectivity of barbiturates against MMP-9.

Conclusion

The *N*-homopiperazine barbiturates included in this study had a reasonable structure–activity relationship and good correlation. The field and Gaussian models were generated and showed good r^2 and q^2 values for Gaussian 3D-QSAR model. The field-based model has $r^2 = 0.845$ and $q^2 = 0.77$ based on the steric and electrostatic fields. The Gaussian model has $r^2 = 0.92$ and $q^2 = 0.85$ based on the five field intensities like Gaussian steric, Gaussian electrostatic, Gaussian HBA, Gaussian HBD, and Gaussian hydrophobic. The analysis of both the 3D-QSAR models indicates that contribution of steric is higher than the other field intensities. The analysis of contour maps for these two models indicate that a molecule with incremental bond length in the 4th position of homopiperazine and piperazine analogs suggests that increased bulk at that position may decrease the activity. This trend is observed even with the hydrophobic intensity. In case of electrostatic, HBA, and HBD, we conclude that HBA and HBD is almost same with all the inhibitors which prevents to establish biological relationship with the interaction established with the receptor MMP-9. The pyrimidine 2,4,6-trione is very much responsible in establishing hydrogen bonds with the Ala 189 and Leu 188, whereas electrostatic field intensity

contribution in the model is very low when compared to other features. Finally, the models developed herein can be further applied for designing of new compounds with potent MMP-9 anticancer activity.

Acknowledgments I acknowledge Dr. Ravi Kumar, Schrodinger for his contribution and guidance to execute the total protocol involved in this study and I convey my gratitude to Mr. Raghu, Schrodinger for his support in completion of this study.

References

Aparna V, Jeevan J, Ravi M, Desiraju GR, Gopalakrishnan B (2006) 3D-QSAR studies on antitubercular thymidine monophosphate kinase inhibitors based on different alignment methods. Bioorg Med Chem Lett 16:1014–1020

Bairy SK, Suneel Kumar BV, Bhalla JU, Pramod AB, Ravikumar M (2009) Three-dimensional quantitative structure–activity relationship studies on c-Src inhibitors based on different docking methods. Chem Biol Drug Des 73:416–427

Chambers AF, Matrisian LM (1997) Changing views of the role of matrix metalloproteinases in metastasis. J Natl Cancer Inst 89: 1260–1270

Cho AE, Guallar V, Berne B, Friesner RA (2005) Importance of accurate charges in molecular docking: quantum mechanical/ molecular mechanical (QM/MM) approach. J Comput Chem 26: 915–931

Georgiadis D, Yiotakis A (2008) Specific targeting of metzincin family members with small-molecule inhibitors: progress toward a multifarious challenge. Bioorg Med Chem 16:8781–8794

Giannelli G, Antonaci S (2002) Gelatinases and their inhibitors in tumor metastasis: from biological research to medical applications. Histol Histopathol 17:339–345

Illemann M, Bird N, Majeed A, Sehested M, Laerum OD, Lund LR, Dano K, Nielsen BS (2006) MMP-9 is differentially expressed in primary human colorectal adenocarcinomas and their metastases. Mol Cancer Res 4:293–302

Jain T, Jayaram B (2007) Computational protocol for predicting the binding affinities of zinc containing metalloprotein–ligand complexes. Proteins 67:1167–1178

Jorgensen WL, Maxwell DS, Tirado-Rives J (1996) Development and testing of the OPLS all-atom force field on conformational energetic and properties of organic liquids. J Am Chem Soc 118:11225–11235

Kim S, Choi MG, Lee HS, Lee SK, Kim SH, Kim WW, Hur SM, Kim JH, Choe JH, Nam SJ, Yang JH, Kim S, Lee JE, Kim JS (2009) Silibinin suppresses TNF-alpha-induced MMP-9 expression in gastric cancer cells through inhibition of the MAPK pathway. Molecules 14:4300–4311

Klein T, Bischoff R (2011) Physiology and pathophysiology of matrix metalloproteases. Amino Acids 41:271–290

Kyaw ZM, Xiang-Qun X (2010) Recent advances in fragment-based QSAR and multi-dimensional QSAR methods. Int J Mol Sci 11:3846–3866

Li Z, Wan H, Shi Y, Ouyang P (2004) Personal experience with four kinds of chemical structure drawing software: review on ChemDraw, ChemWindow, ISIS/Draw, and ChemSketch. J Chem Inf Comput Sci 44:1886–1890

Liu Z, Li L, Yang Z, Luo W, Li X, Yang H, Yao K, Wu B, Fang W (2010) Increased expression of MMP9 is correlated with poor prognosis of nasopharyngeal carcinoma. BMC Cancer 10:270

Loffek S, Schilling O, Franzke CW (2011) Biological role of matrix metalloproteinases: critical balance. Eur Respir J 38:191–208

Marina B, Ivan S (2007) Metastatic cancer cell. Annu Rev Pathol 3:221–247

Murphy G, Knauper V, Atkinson S, Butler G, English W, Hutton M, Stracke J, Clark I (2002) Matrix metalloproteinases in arthritic disease. Arthritis Res 3:S39–S49

Murumkar PR, Zambre VP, Yadav MR (2010) Development of predictive pharmacophore model for insilico screening, 3D QSAR COMFA and COMSIA studies for lead optimization, for designing of potent tumor necrosis factor alpha converting enzyme inhibitors. J Comput Aided Mol Des 24:143–156

Nayana MR, Sekhar YN, Nandyala H, Muttineni R, Bairy SK, Singh K, Mahmood SK (2008) Insight into the structural requirements of proton pump inhibitors based on CoMFA and CoMSIA. J Mol Graph Model 27:233–243

Nuti E, Casalini F, Santamaria S, Gabelloni P, Bendinelli S, Da Pozzo E, Costa B, Marinelli L, LaPietra V, Novellino E, Margarida BM, Fridman R, Da Settimo F, Martini C, Rossello A (2011) Synthesis and biological evaluation in U87MG glioma cells of (ethynyl thiophene) sulfonamide-based hydroxamates as matrix metalloproteinase inhibitors. Eur J Med Chem 46: 2617–2619

Peterson YK, Wang XS, Casey PJ, Tropsha A (2009) Discovery of geranylgeranyltransferase-I inhibitors with novel scaffolds by the means of quantitative structure–activity relationship modeling. Virtual screening and experimental validation. J Med Chem 52:4210–4220

Rao BG (2005) Recent developments in the design of specific matrix metalloproteinase inhibitors aided by structural and computational studies. Curr Pharm Des 11:295–322

Rybakowski JK (2009) Matrix metalloproteinase-9 (MMP9)—a mediating enzyme in cardiovascular disease, cancer, and neuropsychiatric disorders. Cardivasc Psychiatry Neurol 2009:904836

Rybakowski JK, Skibinska M, Kapelski P, Kaczmarek L, Hauser J (2009) Functional polymorphism of the matrix metalloproteinase-9 (MMP-9) gene in schizophrenia. Schizophr Res 109: 90–93

Sabbah DA, Simms NA, Brattain MG, Vennerstrom JL, Zhong H (2012) Biological evaluation and docking studies of recently identified inhibitors of phosphoinositide-3-kinases. Bioorg Med Chem Lett 22:876–880

Schmalfeldt B, Prechtel D, Härting K, Späthe K, Rutke S, Konik E, Fridman R, Berger U, Schmitt M, Kuhn W, Lengyel E (2001) Increased expression of matrix metalloproteinases MMP-2, MMP-9, and the urokinase-type plasminogen activator is associated with progression from benign to advanced ovarian cancer. Clin Cancer Res 7:2396–2404

Singer CF, Kronsteiner N, Marton E, Kubista M, Cullen KJ, Hirtenlehner K, Seifert M, Kubista E (2002) MMP-2 and MMP-9 expression in breast cancer-derived human fibroblasts is differentially regulated by stromal-epithelial interactions. Breast Cancer Res Treat 72:69–77

Tamura Y, Watanable F, Nakatani T, Yasui K, Fuji M, Komurasaki T, Tsuzuki H, Maeskawa R, Yoshioka T, Kawada K, Sugita K, Ohtani M (1998) Highly selective and orally active inhibitors of type IV collagenase (MMP-9 and MMP-2): *N*-sulfonylamino acid derivatives. J Med Chem 41:640–649

Tandon A, Sinha S (2011) Structural insights into the binding of MMP9 inhibitors. Bioinformation 5:310–314

Van den Steen PE, Dubois B, Nelissen I, Rudd PM, Dwek RA, Opdenakker G (2002) Biochemistry and molecular biology of gelatinase B or matrix metalloproteinase-9. Crit Rev Biochem Mol Biol 37:375–536

Verma J, Khedkar VM, Coutinho EC (2010) 3D-QSAR in drug design—a review. Curr Top Med Chem 10:95–115

Wang J, Medina C, Radomski MW, Gilmer JF (2011) *N*-Substituted homopiperazine barbiturates as gelatinase inhibitors. Bioorg Med Chem 19:4985–4999

Weinstat SD, Steeg PS (1994) Angiogenesis and colonization in the tumor metastatic process: basic and applied advances. FASEB J 8:401–407

Zheng S, Chang Y, Hodges KB, Sun Y, Ma X, Xue Y, Williamson SR, Lopez BA, Montironi R, Cheng L (2010) Expression of KISS1 and MMP-9 in non small cell lung cancer and their relations to metastasis and survival. Anticancer Res 30:713–718